

Multuser Interference Mitigation in Noncoherent UWB Ranging via Nonlinear Filtering

Zafer Sahinoglu¹ and Ismail Guvenc²

¹ *Mitsubishi Electric Research Labs, 201 Broadway Avenue, Cambridge, MA 02139, USA*

² *Department of Electrical Engineering, University of South Florida, Tampa, FL 33620, USA*

Received 1 September 2005; Revised 13 April 2006; Accepted 13 June 2006

Ranging with energy detectors enables low-cost implementation. However, any interference can be quite detrimental to range accuracy. We develop a method that performs nonlinear filtering on the received signal energy to mitigate multiuser interference (MUI), and we test it over time hopping and direct sequence impulse radio ultra-wideband signals. Simulations conducted over IEEE 802.15.4a residential line of sight ultrawideband multipath channels indicate that nonlinear filtering helps sustain range estimation accuracy in the presence of strong MUI.

Copyright © 2006 Z. Sahinoglu and I. Guvenc. This is an open access article distributed under the Creative Commons Attribution License, which permits unrestricted use, distribution, and reproduction in any medium, provided the original work is properly cited.

1. INTRODUCTION

In time-of-arrival (ToA)-based ranging, the range accuracy depends heavily on how well the ToA of a signal is estimated. Identifying multipath components and finding the leading path is crucial to decrease ranging errors. With its fractional bandwidth of 20%, or at least 500 MHz bandwidth, an ultra-wideband (UWB) signal provides high time resolution measured in nanoseconds, and UWB helps to separate individual multipath components better than narrowband signals [1].

In UWB ranging, tracking of the leading edge is challenging due to a vast number of multipaths and the fact that the line-of-sight (LoS) path may not have the highest amplitude. Traditionally, UWB approaches based on coherent reception require many rake fingers in order to combine energy from the received signal [2]. However, there is a strong desire to drive down UWB radio cost. This has led to an increased interest in alternative receiver techniques for UWB that do not require the hardware complexity of coherent rake receptions.

One intuitive approach is a trade-off between high performance coherent receivers and low-complexity noncoherent receivers [3]. However, one of the major drawbacks of a noncoherent receiver is its performance in the presence of multiuser interference (MUI). In a multiuser network, signals from multiple devices may interfere with a desired signal and deteriorate the range error drastically. This is because interference suppression techniques such as CDMA are not readily applicable to simple noncoherent receivers. Typically, processing gain is obtained by coherently combining received

signal energy according to transmitted time hopping or DS patterns [4]. However, in coherent energy combining, even a small amount of interference energy may be construed as a leading edge. Therefore, prior to coherent energy combining, it is prudent to remove as much MUI energy as possible.

In this paper, our scope is to make ranging via noncoherent radios resilient to MUI. We focus on simple energy detectors, and propose a MUI mitigation technique for time-hopping impulse radio (TH-IR) [5] and direct sequence impulse radio (DS-IR) UWB systems to sustain submeter range accuracy when MUI is present.

The remainder of this paper is organized as follows. In Section 2, the literature on UWB ranging is reviewed. In Section 3, the TH-IR and DS-IR UWB signal models are given and then the proposed receiver architecture is described. In Section 4, MUI mitigation via nonlinear energy filtering is explained. Section 5 is allocated to the discussion of simulation results. Finally, the paper concludes in Section 6 with a summary of our future work.

2. TOA-BASED UWB RANGING

Acquisition of a signal can be achieved by locking onto the strongest multipath component, which results in a coarse ToA estimate [6–11]. However, precise ToA estimation requires identification of the leading path, which may not be the strongest. In [12], a generalized maximum likelihood (GML) approach is proposed to estimate the leading path by testing the paths prior to the strongest. A stopping rule

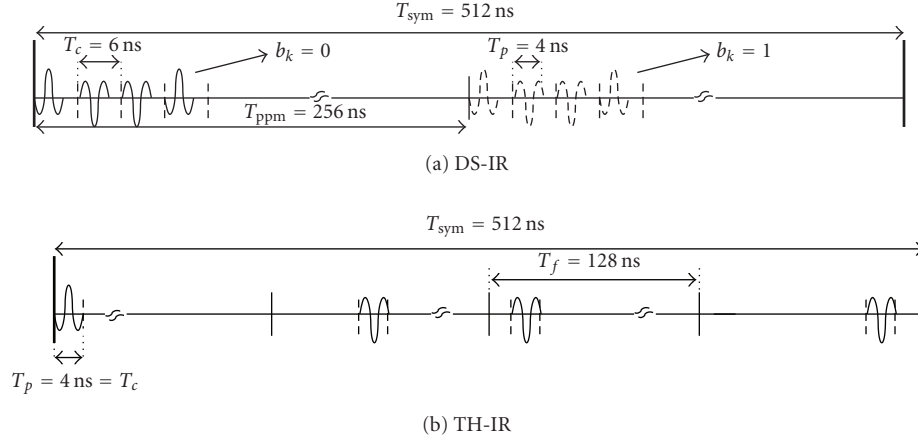


FIGURE 1: Illustration of transmitted waveforms and simulation parameters for (a) DS-IR and (b) TH-IR.

is determined based on the statistics of the amplitude ratio and the delay between the strongest and the leading paths. However, the method requires very high sampling rates on the order of the Nyquist rate. In [13], the authors relax the sampling rate requirements and propose a simpler threshold-based detection technique. In [14], the problem is approached as a break-point estimation for signal presence, where temporal correlation arising from the transmitted pulse is used to accurately partition the received signal.

Acquisition and ToA estimation can generally be achieved by using various transceiver types; for example, matched filters (or stored-reference receivers), transmitted reference receivers, and energy detectors (ED) [6, 15]. The use of energy detectors for synchronization and ToA estimation in UWB systems has been investigated in [15–17]. ED receivers using threshold-based ToA estimation techniques are discussed in [18–20], a multiscale product approach that improves the ranging accuracy was investigated in [21], and likelihood-based techniques are proposed in [15]. Two-step hybrid ToA estimation via ED and matched filters is also studied in [22, 23], where the energy-detection step provides a coarse ToA estimate, and the matched-filtering step refines the estimate. In [24], a matched-filter receiver’s ability to differentiate between the desired user signal and interference for TH-IR UWB during synchronization is analyzed.

Our literature survey indicates that the ToA estimation problem for IR-UWB has been analyzed without consideration of MUI. Note that although MUI mitigation is investigated extensively for IR-UWB systems for symbol detection [25–28], to the best of our knowledge, there is no reference that addresses interference mitigation for ToA estimation with noncoherent UWB radios. This work is intended to fill that gap.

3. RANGING SIGNAL WAVEFORMS AND RECEIVER FRONT-END

In [19], four different waveforms were compared from the ranging perspective. We adopt two of these: DS-IR and

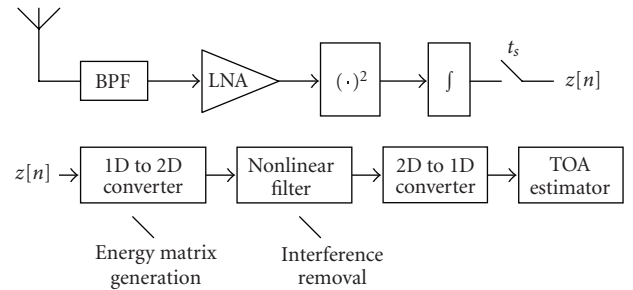


FIGURE 2: Illustration of the energy imaging ranging receiver while processing ED outputs.

TH-IR (see Figure 1), which are currently under consideration for standardization in the IEEE 802.15.4a Task Group.

Each IEEE 802.15.4a packet contains a preamble that consists of multiple repetition of a base symbol waveform; the preamble is used for acquisition/synchronization and ranging. We adopt the IEEE 802.15.4a terminology and use the following notations in the sequel: $E_s^{(k)}$ denotes the symbol energy from the k th user, N_{sym} is the number of symbol repetition within the preamble, ω is the transmitted pulse shape with unit energy, T_{sym} is the symbol duration, T_p is the pulse duration, ϵ_k is the TOA of the k th user’s signal and η is the zero-mean AWGN with variance $\sigma_n^2 = N_0/2$. L_k denotes the total number of multipath components for the k th user, $\gamma_{l,k}$ and $\tau_{l,k}$ represent the amplitude and delay of the l th multipath component for the k th user, respectively, and N_s is the total number of pulses per symbol.

A receiver can process the preamble by either template matching (coherent) or energy detection (ED). Although coherent ranging is superior, the ED receiver offers advantages such as simplicity, operability at sub-Nyquist sampling rates (which determines the range resolution), and low cost. They are also more resilient to pulse-shape distortion.

The ED receiver we study in this paper is illustrated in Figure 2. It first feeds the received signal (after a bandpass filter) into a square-law device, integrates its output, and then

samples periodically. We denote these generated energy samples as $z[n]$, and the sampling interval and the number of samples per symbol as t_s and $n_b = T_{\text{sym}}/t_s$, respectively. The $z[n]$ are then regrouped into a 2D matrix.

Once a matrix is formed, it is passed through a nonlinear filter to enhance desired signal energy parts and remove the MUI. Afterwards, the matrix is converted back to 1D time series to locate the leading edge, by means of adaptive search-back and threshold techniques. In what follows, we present signal models for DS-IR and TH-IR systems.

3.1. DS-IR

In DS-IR, a symbol interval is divided into two halves. A group of closely spaced pulses called *burst* is transmitted either in the first or the second half in a pseudorandom pattern. With such an orthogonal burst positioning, ranging can be performed in the presence of multiple simultaneously operating devices. The received DS-IR symbol waveform from user k can be written as

$$\omega_{\text{mp},k}^{(\text{ds})}(t) = \sqrt{\frac{E_s^{(k)}}{N_s}} \sum_{l=1}^{L_k} \gamma_{l,k} \sum_{j=1}^{N_s} d_{j,k}^{(\text{ds})} \times \omega(t - (j-1)T_c^{(\text{ds})} - \tau_{l,k} - \epsilon_k), \quad (1)$$

where $d_{j,k}^{(\text{ds})} \in \{\pm 1\}$ are the binary sequences for the k th user, and $T_c^{(\text{ds})}$ is the chip duration (pulse repetition interval) such that $T_c^{(\text{ds})} \geq T_p$. The polarities of the pulses in a burst are used to convey data for coherent reception. Therefore, the spacing between the pulses enables coherent receivers to demodulate the data.

If there are K simultaneously transmitting users, the received signal would be

$$r^{(\text{ds})}(t) = \sum_{k=1}^K \sum_{\lambda=1}^{N_{\text{sym}}} \omega_{\text{mp},k}^{(\text{ds})}(t - \lambda T_{\text{sym}} - b_{\lambda,k} T_{\text{ppm}}) + \eta(t), \quad (2)$$

where $b_{\lambda,k} \in \{0, 1\}$ is the λ th symbol of k th user, and T_{ppm} is the modulation index (i.e., delay) for pulse-burst position modulation (PPM). Note that varying T_{ppm} would change the interburst interval. Hence, multiple orthogonal waveforms can be generated, and each can be assigned to users of different networks.

The ED output samples at the desired receiver with the DS-IR waveforms is

$$z^{(\text{ds})}[n] = \int_{(n-1)t_s}^{nt_s} |r^{(\text{ds})}(t)|^2 dt, \quad (3)$$

where $n = 1, 2, \dots, N_b$, and $N_b = N_{\text{sym}} n_b$.

3.2. TH-IR

In TH-IR, a symbol is divided into virtual time intervals T_f called *frames*, which is further decomposed into smaller time slots $T_c^{(\text{th})}$ called *chips*. A single pulse is transmitted in each frame on a chip location specified by a user-specific pseudo-random time-hopping code. The received TH-IR signal from

user k is

$$\omega_{\text{mp},k}^{(\text{th})}(t) = \sqrt{\frac{E_s^{(k)}}{N_s}} \sum_{l=1}^{L_k} \gamma_{l,k} \sum_{j=1}^{N_s} d_{j,k} \times \omega(t - (j-1)T_f - c_{j,k}T_c - \tau_{l,k} - \epsilon_k), \quad (4)$$

where $c_{j,k}$ and $d_{j,k}$ are the TH codes and polarity scrambling codes of user k , respectively. If K users are transmitting N_{sym} symbols simultaneously, each with a unique TH code, the received signal by the desired user becomes

$$r^{(\text{th})}(t) = \sum_{k=1}^K \sum_{\lambda=1}^{N_{\text{sym}}} \omega_{\text{mp},k}^{(\text{th})}(t - \lambda T_{\text{sym}}) + \eta(t). \quad (5)$$

The collected energy samples at the ED receiver would be

$$z^{(\text{th})}[n] = \int_{(n-1)t_s}^{nt_s} |r^{(\text{th})}(t)|^2 dt. \quad (6)$$

3.3. Conventional energy combining (Conv)

A conventional receiver coherently combines the energies over N_{sym} symbols to improve the signal-to-noise ratio (SNR) using the bit sequence of the desired user in the DS-IR case,¹ and over $N_{\text{sym}} \times N_s$ pulse positions using the TH sequences of the desired user in the TH-IR case. Then, a search-back algorithm is applied to locate the leading signal energy.

In this paper, we adopt the searchback scheme presented in [19]. With the assumption that the receiver is perfectly synchronized to the strongest energy sample, the algorithm tries to identify the leading edge by searching the samples backward within a predetermined window starting from the strongest sample. In non-LoS environments, the strongest path may arrive as much as 60 ns after the first path [29]. At 4 ns sampling period, this would correspond to 15 samples. Therefore, in the searchback algorithm (see Algorithm 1), it would be sufficient to have $W = 15$.

Each sample within the searchback window is compared to a threshold. Even if it is smaller than the threshold, the algorithm does not terminate; and it allows up to w_{cls} consecutive noise-only samples. This is because clustering of the multipath components yields noise-only regions between the clusters. The threshold ξ that corresponds to a fixed P_{fa} is given by² [19]

$$\xi = \sigma_{\text{ed}} Q^{-1}(1 - (1 - P_{\text{fa}})^{1/w_{\text{cls}}}) + \mu_{\text{ed}}, \quad (7)$$

where μ_{ed} and σ_{ed} are the mean and the variance of noise-only samples. The optimal threshold is a function of w_{cls} .

¹ For DS-IR, we assume that we do not combine energies from different pulses within the same symbol in order to avoid weakening the leading edge due to multipath effects [19].

² We define P_{fa} to be the probability of identifying a noise-only sample as a signal sample.

```

 $n_{\max}$  : the index of the strongest energy sample,
 $n_{\text{le}}$  := the index of the first signal energy sample,
 $W$  : the searchback window length,
 $\xi$  := noise-based threshold,
Let  $i = n_{\max}, w_{\text{cls}} = 2$ ,
while  $i \geq n_{\max} - W$ 
  if  $z[i] \geq \xi$  or  $z[i-1] \geq \xi$  or  $z[i-2] \geq \xi$ ,  $i = i - 1$ ,
  else
    break,
  endif
endwhile
Return  $n_{\text{le}} = i + 1$ .

```

ALGORITHM 1: Pseudocode for the adaptive searchback algorithm to locate the leading signal energy.

4. ENERGY MATRIX FORMATION

SNR is one of the parameters that range estimation accuracy heavily depends on. Although the SNR can be improved via processing gain by coherently combining received signal energy samples [22], Figure 3 illustrates poor ranging performance after coherent energy combining in the presence of MUI. In the given TH-IR example, the symbol consists of four frames with signal energy integrated and sampled at a period that produces four energy samples in each frame and 16 samples in total per symbol. The TH code of the desired signal is $\{0, 4, 4, 3\}$, and that of the interference is $\{0, 4, 5, 4\}$. Coherent combining requires energy samples $z[n]$ of the received signal to be combined in accordance with the matched TH code. Figure 3 produces the combined energy values $E[n]$ such that $E[n] = z[n+0] + z[n+4] + z[n+4+4] + z[n+4+4+3]$, where $0 \leq n \leq 3$, assuming that TOA ambiguity is as much as the frame duration. If there is no interference, $E[1] = 4A$ and $E[n] = 0$ for $n \neq 1$ and the TOA index is 1. In the presence of interference, the time of arrival information is very likely impacted, and it is easy to see in the example that TOA index becomes 0 because $E[0] = 2A$ (see Figure 3(d)).

We have now illustrated that signal design itself and coherent energy combining is not sufficient to deal with the detrimental impact of interference. A solution simply lies in considering the collected energy samples from a different view: a two-dimensional energy matrix. Let us create a so-called energy matrix \mathbf{Z} of size $M \times N$, where M is the number of frames processed and N the number of energy samples collected from each frame. Referring to the previous example, the size of \mathbf{Z} would be 4×4 and populated as follows:

$$\mathbf{Z} = \begin{pmatrix} z[0+11] & z[1+11] & z[2+11] & z[3+11] \\ z[0+8] & z[1+8] & z[2+8] & z[3+8] \\ z[0+4] & z[1+4] & z[2+4] & z[3+4] \\ z[0+0] & z[1+0] & z[2+0] & z[3+0] \end{pmatrix}. \quad (8)$$

Filling out each column of \mathbf{Z} with samples grouped according to the received signal's TH pattern forms vertical lines whenever signal energy is present in all of those samples (Figure 3(e)). The detection of the left-most vertical line

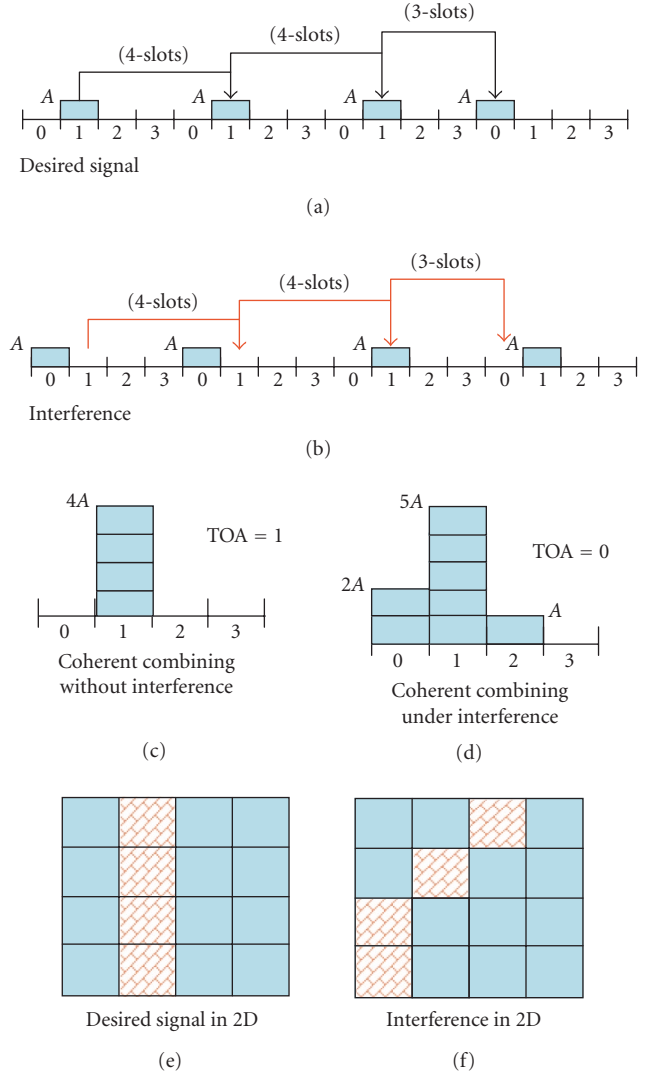


FIGURE 3: Illustration of coherent energy combining in 1D (a) energy samples from TH-IR desired user, (b) energy samples from TH-IR interference, (c) coherent combining of energy samples without interference, (d) coherent combining of energy samples with interference, (e) energy image of the desired signal, \mathbf{Z} , and (f) energy image of the interference.

gives the time index of the first arriving signal energy. If the interference follows a different TH pattern, intuitively the energy matrix of the interference does not form a vertical line (Figure 3(f)).

Conv does not account for the MUI, and it directly aggregates the energy samples. This is equivalent to summing the rows of \mathbf{Z} along each column, yielding an energy vector. Note that the column sum of the matrix in Figure 3(e) generates the energy vector in Figure 3(c), and column-sum of (e) + (f) results in Figure 3(d).

Applying conventional leading edge detection techniques on the energy vector in Figure 3(d) causes erroneous ranging due to interference. It is clear from the illustrations that the energy matrix provides an insight into the presence and

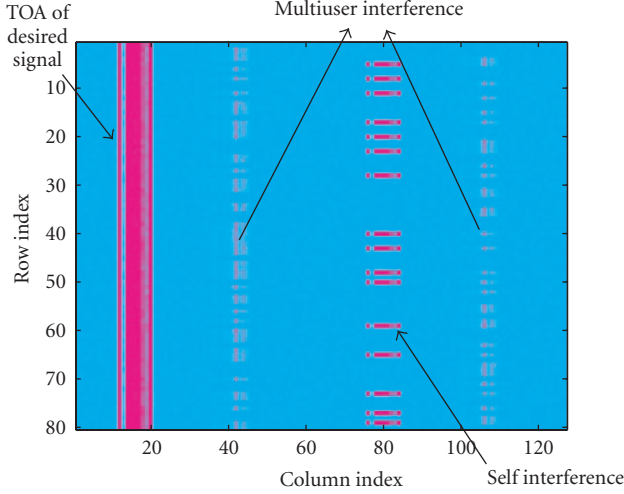


FIGURE 4: Energy image for the DS-IR ($E_b^{(\text{des})}/N_0 = 16$ dB, $E_b^{(\text{int})}/N_0 = 10$ dB, $t_c = 4$ ns, $N_s = 4$, $T_{\text{sym}} = 512$ ns, $T_{\text{ppm}} = 256$ ns, $n_b = 128$). The row index corresponds to symbols and the column index corresponds to the samples within a symbol interval.

whereabout of interference energy, and nonlinear filters can be applied onto the matrix to mitigate this interference. The following subsections explain how to form an energy matrix from DS-IR and TH-IR waveforms.

4.1. Energy matrix of DS-IR

Let λ denote the row index (which is also the symbol index), and κ denote the column index of the matrix. Then, the samples in (3) can be used to populate the matrix as follows:

$$\mathbf{Z}^{(\text{ds})}[\lambda, \kappa] = \mathbf{z}^{(\text{ds})} \left[\kappa + (\lambda - 1)n_b + b_{\lambda,1} \frac{T_{\text{ppm}}}{t_s} \right], \quad (9)$$

where $1 \leq \lambda \leq N_{\text{sym}}$ and $1 \leq \kappa \leq n_b$.

A typical energy matrix of a DS-IR signal after passing through an IEEE 802.15.4a CM1 channel is given in Figure 4 while the E_b/N_0 is 16 dB for the desired received signal and 10 dB for the interference. Clearly, the desired signal forms a vertical line indicating multipath components, whereas the interference pattern is intermittent.

Self-interference may also be present in the energy matrix. This occurs when only some of the samples of a column actually overlap with the energy from bursts.

The energy vector $\tilde{\mathbf{z}}^{(\text{ds})}$ that the *Conv* receiver generates is equivalent to the column-sum of $\mathbf{Z}^{(\text{ds})}$,

$$\tilde{\mathbf{z}}^{(\text{ds})} = \mathbf{1}_{N_{\text{sym}}} \mathbf{Z}^{(\text{ds})}, \quad (10)$$

where $\mathbf{1}_{N_{\text{sym}}}$ is a row vector of all ones.

4.2. Energy matrix of TH-IR

In TH-IR, energy samples given in (6) are grouped together according to the transmitted TH code, and samples of the same group are used to populate a column of the energy

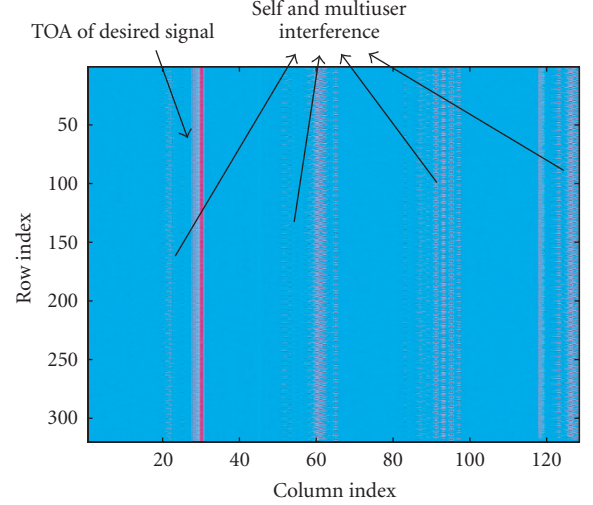


FIGURE 5: Energy image for the TH-IR ($E_b^{(\text{des})}/N_0 = 16$ dB, $E_b^{(\text{int})}/N_0 = 10$ dB, $t_c = 4$ ns, $N_s = 4$, $T_{\text{sym}} = 512$ ns, $T_f = 128$ ns, $n_b = 128$).

matrix $\mathbf{Z}^{(\text{th})}$. As a result, there are $N_s \times N_{\text{sym}}$ rows,

$$\mathbf{Z}^{(\text{th})}[\lambda(j), \kappa] = \mathbf{z}^{(\text{th})} \left[\kappa + (\lambda - 1)n_b + j \frac{T_f}{t_s} + c_{j,1} \frac{T_c}{t_s} \right], \quad (11)$$

where $\lambda(j) = N_s(\lambda - 1) + j$, and $j \in \{1, 2, \dots, N_s\}$. We assume that T_c is an integer multiple of t_s to allow the collection of the energies over integer number of pulses.

A typical energy matrix of a TH-IR signal after passing through an IEEE 802.15.4a CM1 channel is given in Figure 5. The E_b/N_0 is 16 dB for the desired received signal and 10 dB for the interference. Note that MUI and self-interference causes short discrete lines. The actual ToA corresponds to the left-most continuous vertical line in $\mathbf{Z}^{(\text{th})}$.

A cause of the self-interference is the imperfect autocorrelation of the TH codes. Note that the energy samples of a column are grouped according to the desired user's TH code. It is possible that only some of the grouped samples contain energy from the received signal due to a partial overlap with the signal's TH pattern. Especially if the uncertainty region for the ToA is larger than T_f , the energy collection process would cause more self-interference. Nonlinear filters would not be able to distinguish self-interference from MUI.

Furthermore, to suppress noise N_{img} matrices can be superposed, relying on the assumption that the statistics of interference and noise are stationary. The *Conv* would column-sum $\mathbf{Z}^{(\text{th})}$ and would perform edge detection on $\tilde{\mathbf{z}}^{(\text{th})}$,

$$\tilde{\mathbf{z}}^{(\text{th})} = \mathbf{1}_{N_s N_{\text{sym}}} \mathbf{Z}^{(\text{th})}. \quad (12)$$

5. NONLINEAR MATRIX FILTERING

In this section, we consider two nonlinear filters for interference mitigation: minimum filter and median filter. In the following discussion, without losing generality, we drop the

superscript of the energy matrix for DS-IR and TH-IR, and refer to it as \mathbf{Z} .

5.1. Minimum filter: *min*

To remove outliers in \mathbf{Z} , which are most likely due to interference, we apply length W minimum filter along each column. The minimum filter replaces the center sample with the minimum of the samples within the filter window. Then, the elements of the new energy matrix $\mathbf{Z}^{(\min)}$ become

$$\begin{aligned} \mathbf{Z}^{(\min)}[\lambda, \kappa] \\ = \min \left\{ \mathbf{Z}[\lambda, \kappa], \mathbf{Z}[\lambda + 1, \kappa], \dots, \mathbf{Z}[\lambda + W - 1, \kappa] \right\}, \end{aligned} \quad (13)$$

where $\lambda \in \{1, 2, \dots, N_{\text{sym}} - W + 1\}$ for DS-IR and $\lambda \in \{1, 2, \dots, N_s N_{\text{sym}} - W + 1\}$ for TH-IR. Once the interference is removed, $\mathbf{Z}^{(\min)}$ is converted to a vector by the column-sum operation,

$$\begin{aligned} \tilde{\mathbf{z}}^{(\text{ds}, \min)} &= \mathbf{1}_{N_{\text{sym}} - W + 1} \mathbf{Z}^{(\text{ds}, \min)}, \\ \tilde{\mathbf{z}}^{(\text{th}, \min)} &= \mathbf{1}_{N_s N_{\text{sym}} - W + 1} \mathbf{Z}^{(\text{th}, \min)}, \end{aligned} \quad (14)$$

where $\mathbf{Z}^{(\text{ds}, \min)}$ indicates *Min* filtered matrix for the DS-IR and $\mathbf{Z}^{(\text{th}, \min)}$ for the TH-IR. Note that while it significantly removes the interference, the *Min* filter may also degrade the desired signal.

5.2. Median filter: *median*

Median filters are special cases of stack filters that have been widely used in digital image and signal processing [30, 31] to remove singularities caused by noise. A median filter replaces the center value in a given data set with the median of the set. A longer median filter makes output noise more colored and is less effective to mitigate interference because any unsuppressed interference energy may propagate onto its neighboring samples. We use a length 3 median filter in our simulations and refer to it as *Median*. One way to prevent coloring of output noise is to apply the median filter in nonoverlapping windows. In the appendix, we quantify the impact of nonoverlapping median filtering on detection performance of DC signals in white Gaussian noise to provide some insight into more complex detection problems. In (15), $\mathbf{Z}^{(\text{med})}$ is the energy matrix at the output of the median filter,

$$\begin{aligned} \mathbf{Z}^{(\text{med})}[\lambda, \kappa] \\ = \text{median} \left\{ \mathbf{Z}[\lambda, \kappa], \mathbf{Z}[\lambda + 1, \kappa], \dots, \mathbf{Z}[\lambda + W - 1, \kappa] \right\}. \end{aligned} \quad (15)$$

After converting $\mathbf{Z}^{(\text{med})}$ into an energy vector, we have

$$\begin{aligned} \tilde{\mathbf{z}}^{(\text{ds}, \text{med})} &= \mathbf{1}_{N_{\text{sym}} - W + 1} \mathbf{Z}^{(\text{ds}, \text{med})}, \\ \tilde{\mathbf{z}}^{(\text{th}, \text{med})} &= \mathbf{1}_{N_s N_{\text{sym}} - W + 1} \mathbf{Z}^{(\text{th}, \text{med})}. \end{aligned} \quad (16)$$

The leading edge search is performed on $\tilde{\mathbf{z}}^{(\text{ds}, \text{med})}$ for DS-IR waveforms and on $\tilde{\mathbf{z}}^{(\text{th}, \text{med})}$ for TH-IR waveforms.

Note that both minimum and median filtering add to the (low) complexity of an energy-detection receiver. Assume that $z[n]$ are provided by a 16-bit ADC. Then, the memory requirement for storing \mathbf{Z} of size $M \times N$ would be $2MN$ bytes. It is known that sorting W numerals has an inherent computational complexity of $O(W \log W)$. Thus, the overall complexity of applying *Median* or *Min* would be $M(N - W + 1)O(W \log W)$.

6. SIMULATION RESULTS

The DS-IR and TH-IR signals are transmitted over IEEE 802.15.4a CM1 (residential line-of-sight) channels. For performance comparison, we use mean absolute error (MAE) of ToA estimations over 1000 realizations. DS-IR and TH-IR symbol waveforms of length 512 ns are considered; the other simulation settings are as follows: $T_{\text{sym}} = 512$ ns, $T_{\text{ppm}} = 256$ ns, $T_f = 128$ ns, $T_p = 4$ ns, $w_{\text{cls}} = 2$, and $T_c = 4$ ns for TH-IR and 6 ns for DS-IR, and the integration interval is 4 ns. Energy images are obtained using 80 symbols (yielding 80 rows for DS-IR, and 320 rows for TH-IR), and the images are further assumed to be averaged over 250 realizations.³ For TH-IR, the time-hopping sequence for the desired user is $c_{j,1} = [1, 1, 4, 2]$, and for the interfering user $c_{j,2} = [1, 4, 2, 1]$, where there are $T_f/T_c = 64$ chip positions per frame.⁴

We compare the ranging accuracy of the searchback algorithm described in Algorithm 1 under different interference levels. Let $E^{(1)}$ and $E^{(2)}$ denote the symbol energies received from the desired user and the interfering user, respectively (we also use E_b for the desired user's bit energy). Then, we simulate the interference levels, where $E^{(2)}/N_0 \in \{-\infty, 0, 5, 10\}$ dB. Energy matrices are constructed, and MAEs before (*Conv*) and after nonlinear filtering (*Min*, *Median*) are obtained for all cases using a nonlinear filter window length of 3.

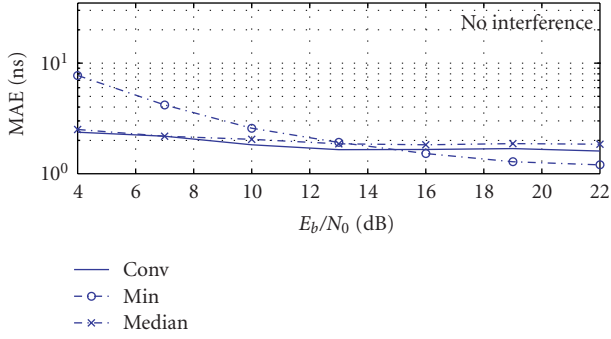
6.1. DS-IR

The MAE results in Figure 6(a) show that in the absence of MUI, the *Conv* and *Median* outperforms *Min* by achieving MAE as low as 2 ns at E_b/N_0 values less than 14 dB. This makes sense intuitively, because when noise is the dominant term, *Min* penalizes the signal.

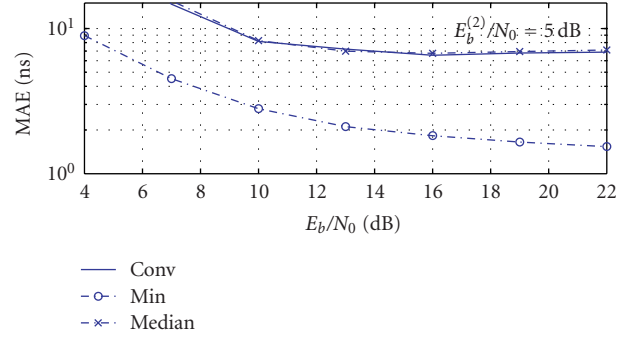
However, at higher E_b/N_0 , the MAE of *Min* is better than those of both *Conv* and *Median*, because at high E_b/N_0 , self-interference becomes the dominant factor, and (for certain channel realizations) the multipath components from a previous symbol may extend into the searchback window and still degrade the ranging accuracy of *Conv* and *Median* (see Figure 4). Minimum filtering remains effective to mitigate self-interference at high SNRs.

³ We assume that the bit sequences used in DS-IR repeat at every 80 symbols; the total preamble length considered for ranging purposes is therefore $512 \times 80 \times 250 \approx 10$ ms.

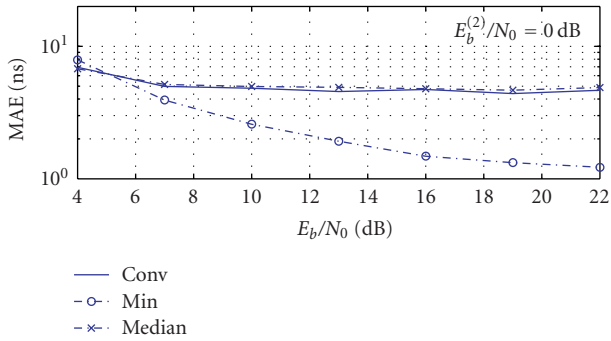
⁴ These sequences are obtained using a brute-force computer search so that they have a zero correlation zone larger than 100 ns.



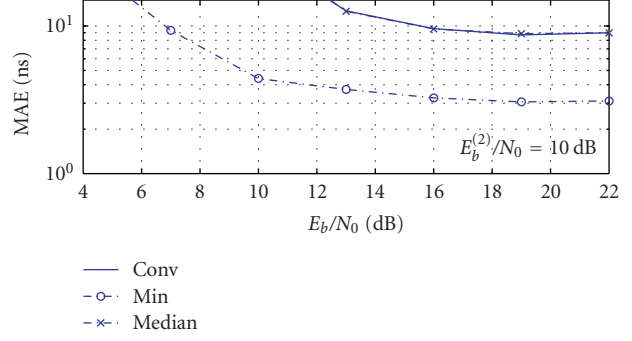
(a)



(a)



(b)



(b)

FIGURE 6: MAEs for DS-IR: (a) no interference, and (b) $E_b^{(2)}/N_0 = 0$ dB ($w_{cls} = 2$).

FIGURE 7: MAEs for DS-IR: (a) $E_b^{(2)}/N_0 = 5$ dB, and (b) $E_b^{(2)}/N_0 = 10$ dB ($w_{cls} = 2$).

The MAEs of the three approaches at $E^{(2)}/N_0 \in \{0, 5, 10\}$ dB are presented in Figures 6(b), 7(a), and 7(b), respectively. The MAE error floors of *Conv* and *Median* are approximately 5 ns, 7 ns, and 9 ns at interference levels of 0 dB, 5 dB, and 10 dB, respectively. Whereas, *Min* provides a much smaller error floor. When $E^{(2)}/N_0 = 0$ dB and $E^{(1)}/N_0$ is higher than 9 dB, *Min* can achieve the MAE of 3 ns (sub-meter range accuracy). *Min* requires at least $E^{(1)}/N_0 = 10$ dB at $E^{(2)}/N_0 = 5$ dB to keep the MAE below 3 ns, and $E^{(1)}/N_0 = 16$ dB at $E^{(2)}/N_0 = 10$ dB.

6.2. TH-IR

In general, the TH-IR waveform yields higher MAEs when compared to the DS-IR for the simulated set of parameters. This can be explained by higher self-interference from autocorrelation sidelobes of TH-IR waveforms; although TH sequences with a large zero correlation zones are used in our simulations, for the channels with large maximum excess delays, the performance is degraded. In the DS-IR case, *Min* effectively suppresses self-interference even at high E_b/N_0 .

An interesting observation with TH-IR waveforms is that there exists an optimum E_b/N_0 and the MAE starts increasing beyond the optimum even if there is no MUI, because increasing the E_b/N_0 also increases the energy of autocorrelation sidelobes; since threshold is set based only on the noise

level, stronger self-interference starts degrading the performance after the optimum SNR level.⁵

In the presence of interference, the MAEs of the three approaches at $E^{(2)}/N_0 \in \{0, 5, 10\}$ dB are presented in Figures 8(b), 9(a), and 9(b), respectively.

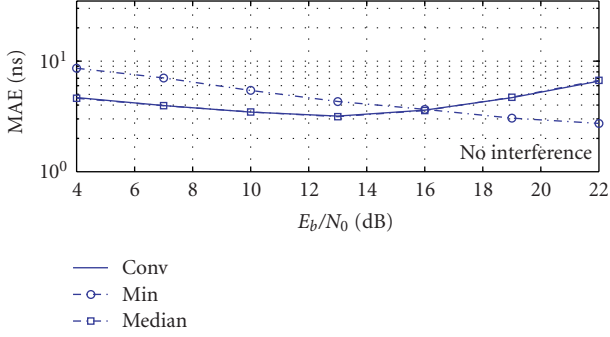
The presence of interference at levels of $E^{(2)}/N_0 = 0$ dB or higher drastically impacts the performance of *Conv* and *Median* and as a result their MAE never falls below 6 ns, whereas the MAE of *Min* remains the same as the no-interference case when $E^{(2)}/N_0 = \{0, 5\}$ dB. Even when $E^{(2)}/N_0 = 10$ dB, the MAE floor of the *Min* approaches 5 ns at very high SNR ($E^{(1)}/N_0 = 18$ dB).

These results suggest that better searchback and threshold techniques need to be developed for the TH-IR case to obtain more accurate ranging. Also, the energy matrix with minimum filtering proves to be effective to deal with interference in the TH-IR case.

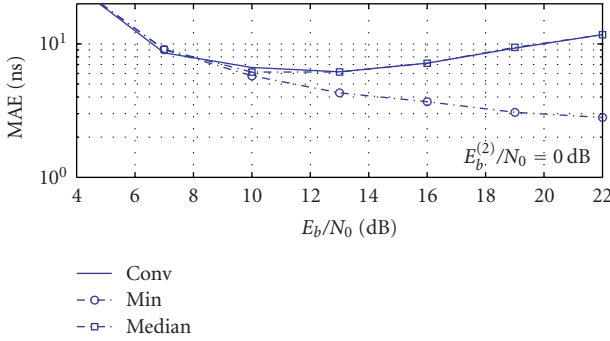
7. CONCLUSION

In this paper, we introduce a ranging method that uses a matrix of received energy samples from a square-law device,

⁵ The searchback algorithm in Algorithm 1 continues to iterate due to multipath interference rather than terminating at the leading edge.



(a)



(b)

FIGURE 8: MAEs for TH-IR: (a) no interference, and (b) $E_b^{(2)}/N_0 = 0$ dB ($w_{\text{cls}} = 2$).

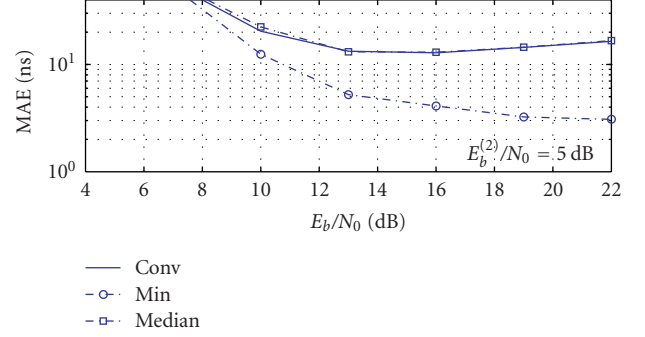
and applies nonlinear filtering to the matrix to remove outliers caused by interference. The nonlinear minimum filter is recommended based on our simulation results. After the nonlinear filtering, energy values along each column of the matrix are aggregated. Hence, the two-dimensional data are converted into an energy vector. Then, a searchback algorithm is run on the energy vector to locate the leading signal energy.

The effectiveness of this approach is proven by simulations conducted using IEEE 802.15.4a channel models. Nonlinear filtering changes noise and signal characteristics. Due to space limitations, the impact of nonlinear filtering on the receiver detection performance will be studied in a separate article.

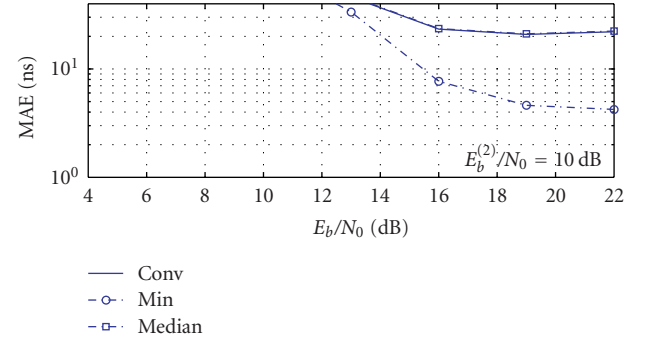
This study reveals the following.

- (i) Ranging is quite sensitive to interference, since the leading edge sample may be very weak compared to interference samples.
- (ii) A single interference energy sample may prolong the searchback process, and increase ranging error.
- (iii) In addition to multiuser interference, the searchback algorithm must handle self-interference.

Finally, we present a framework and provide practical algorithms to mitigate multiuser interference in ToA estimation via noncoherent ultra-wideband systems. Our future work includes development of adaptive algorithms (e.g., minimum and median filters with adaptive window size) for



(a)



(b)

FIGURE 9: MAEs for TH-IR: (a) $E_b^{(2)}/N_0 = 5$ dB, and (b) $E_b^{(2)}/N_0 = 10$ dB ($w_{\text{cls}} = 2$).

enhanced ranging accuracy under varying levels of interference, and quantification of the impact of nonlinear filtering on detection performance.

APPENDIX

Consider the problem of detecting a DC level in a known Gaussian noise source, and assume that the noise distribution has zero mean and variance σ^2 . Assume that there are N i.i.d. observations of the test data $z[n]$. When there is no signal, the data set belongs to a noise only hypothesis H_0 , and when signal is present it belongs to hypothesis H_1 ,

$$\begin{aligned} H_0 : \mathbf{z}[n] &= w[n], \quad n = 1, 2, \dots, N, \\ H_1 : \mathbf{z}[n] &= A + w[n], \quad n = 1, 2, \dots, N. \end{aligned} \quad (\text{A.1})$$

The probability of detection, P_D , with the Neyman-Pearson detector for this problem is given in [32] as

$$P_D = Q\left(Q^{-1}(P_{\text{FA}}) - \sqrt{\frac{NA^2}{\sigma_n^2}}\right). \quad (\text{A.2})$$

Note that after length W median filtering with nonoverlapping windows, the new observation set would have only N/W samples and the noise variance would be scaled by $f(W)$, where $f(\cdot)$ indicates a function. Since the input distribution is Gaussian, the output would approximate to Gaussian with the same mean, but lower variance [33].

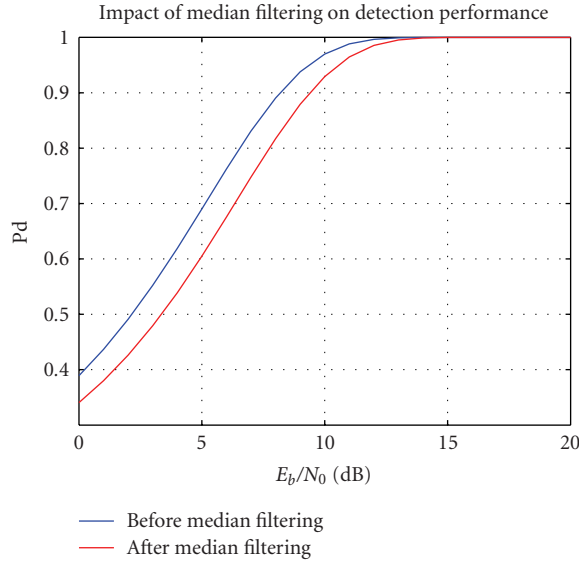


FIGURE 10: Degradation in probability of detection after length 3 median filtering for “DC level detection in Gaussian noise” problem. Here $W = 3$, $f(3) = 0.44$. Note that median filtering with nonoverlapping windows degrades detection performance.

Theoretically, the output density of the length 3 median filter is

$$p_2(y) = 6Q_z(y)(1 - Q_z(y))p_z(y), \quad (\text{A.3})$$

where Q_z is the complementary cumulative distribution function and $p_z(y)$ is the density of the input data. Our numerical analysis indicates that $f(3) = 0.44$ providing a close approximation to (A.3). The Kolmogorov-Smirnow test to compare the approximated density function and (A.3) results in the significance level of 0.1%. Then, in consideration of the approximation, the probability of detection P_D^m after median filtering becomes

$$P_D^m = Q\left(Q^{-1}(P_{FA}) - \sqrt{\frac{(N/W)A^2}{f(W) \times \sigma_n^2}}\right). \quad (\text{A.4})$$

Here, the problem of detecting a DC level in Gaussian noise is addressed for its simplicity, and Figure 10 shows that median filtering in nonoverlapping windows would lower the probability of detection. If the length 3 median filter is applied with two-sample overlapping windows, the output noise would be a colored Gaussian, but the size of the observation set would remain N . It may be possible to observe an increase in detection performance. Quantification of the impacts of median filtering with overlapping windows on the detection performance of noncoherent receivers will be studied in detail in our future work.

ACKNOWLEDGMENTS


The authors wish to thank Dr. Philip Orlik and Dr. Andy F. Molisch for their beneficial feedback and comments during the course of this work. We also thank our anonymous reviewers for their help to improve this presentation.

REFERENCES

- [1] Z. Tarique, W. Q. Malik, and D. J. Edwards, “Bandwidth requirements for accurate detection of direct path in multipath environment,” *Electronics Letters*, vol. 42, no. 2, pp. 100–102, 2006.
- [2] M. Z. Win, G. Chrisikos, and N. R. Sollenberger, “Performance of Rake reception in dense multipath channels: implications of spreading bandwidth and selection diversity order,” *IEEE Journal on Selected Areas in Communications*, vol. 18, no. 8, pp. 1516–1525, 2000.
- [3] J. Ellis, et al., “IEEE P802.15.4a WPAN alternate PHY - PAR,” January, 2004, doc.: IEEE 802.15-04/048r1. <http://www.ieee802.org/15/pub/TG4a.html>.
- [4] S. Gezici, Z. Tian, G. B. Giannakis, et al., “Localization via ultra-wideband radios: a look at positioning aspects of future sensor networks,” *IEEE Signal Processing Magazine*, vol. 22, no. 4, pp. 70–84, 2005.
- [5] M. Z. Win and R. A. Scholtz, “Impulse radio: how it works,” *IEEE Communications Letters*, vol. 2, no. 2, pp. 36–38, 1998.
- [6] L. Reggiani and G. M. Maggio, “Rapid search algorithms for code acquisition in UWB impulse radio communications,” *IEEE Journal on Selected Areas in Communications*, vol. 23, no. 5, pp. 898–908, 2005.
- [7] J. Yu and Y. Yao, “Detection performance of time-hopping ultrawideband LPI waveforms,” in *Proceedings of IEEE Sarnoff Symposium*, Princeton, NJ, USA, April 2005.
- [8] Z. Tian and G. B. Giannakis, “A GLRT approach to data-aided timing acquisition in UWB radios—part I: algorithms,” *IEEE Transactions on Wireless Communications*, vol. 4, no. 6, pp. 2956–2967, 2005.
- [9] Z. Tian and G. B. Giannakis, “A GLRT approach to data-aided timing acquisition in UWB radios—part II: training sequence design,” *IEEE Transactions on Wireless Communications*, vol. 4, no. 6, pp. 2994–3004, 2005.
- [10] W. Chung and D. Ha, “An accurate ultra wideband (UWB) ranging for precision asset location,” in *Proceedings of IEEE Conference on Ultra Wideband Systems and Technologies (UWBST '03)*, pp. 389–393, Reston, Va, USA, November 2003.
- [11] R. Fleming, C. Kushner, G. Roberts, and U. Nandiwada, “Rapid acquisition for ultra-wideband localizers,” in *Proceedings of IEEE Conference on Ultra Wideband Systems and Technologies (UWBST '02)*, pp. 245–249, Baltimore, Md, USA, May 2002.
- [12] J.-Y. Lee and R. A. Scholtz, “Ranging in a dense multipath environment using an UWB radio link,” *IEEE Journal on Selected Areas in Communications*, vol. 20, no. 9, pp. 1677–1683, 2002.
- [13] R. A. Scholtz and J.-Y. Lee, “Problems in modeling UWB channels,” in *Proceedings of IEEE Conference Record of the Asilomar Conference on Signals, Systems and Computers*, vol. 1, pp. 706–711, Pacific Grove, Calif, USA, November 2002.
- [14] C. Mazzucco, U. Spagnolini, and G. Mulas, “A ranging technique for UWB indoor channel based on power delay profile analysis,” in *Proceedings of IEEE 59th Vehicular Technology Conference (VTC '04)*, vol. 5, pp. 2595–2599, Milan, Italy, May 2004.
- [15] I. Guvenc and Z. Sahinoglu, “TOA estimation with different IR-UWB transceiver types,” in *Proceedings of IEEE International Conference on Ultra-Wideband (ICU '05)*, pp. 426–431, Zurich, Switzerland, September 2005.
- [16] A. Rabbachin and I. Oppermann, “Synchronization analysis for UWB systems with a low-complexity energy collection receiver,” in *Proceedings of International Workshop on Ultra Wideband Systems; Joint with Conference on Ultra Wideband*

- Systems and Technologies*, pp. 288–292, Kyoto, Japan, May 2004.
- [17] K. Yu and I. Oppermann, “Performance of UWB position estimation based on time-of-arrival measurements,” in *Proceedings of International Workshop on Ultra Wideband Systems; Joint with Conference on Ultra Wideband Systems and Technologies*, pp. 400–404, Kyoto, Japan, May 2004.
- [18] I. Guvenc and Z. Sahinoglu, “Threshold-based TOA estimation for impulse radio UWB systems,” in *Proceedings of IEEE International Conference on Ultra-Wideband (ICU ’05)*, pp. 420–425, Zurich, Switzerland, September 2005.
- [19] I. Guvenc, Z. Sahinoglu, A. F. Molisch, and P. Orlik, “Non-coherent TOA estimation in IR-UWB systems with different signal waveforms,” in *Proceedings of 1st IEEE/CreateNet International Workshop on Ultrawideband Wireless Networking (UWBNETS ’05)*, pp. 245–251, Boston, Mass, USA, July 2005, (invited paper).
- [20] I. Guvenc and Z. Sahinoglu, “Threshold selection for UWB TOA estimation based on kurtosis analysis,” *IEEE Communications Letters*, vol. 9, no. 12, pp. 1025–1027, 2005.
- [21] I. Guvenc and Z. Sahinoglu, “Multiscale energy products for TOA estimation in IR-UWB systems,” in *Proceedings of IEEE Global Telecommunications Conference (GLOBECOM ’05)*, vol. 1, pp. 209–213, St. Louis, Mo, USA, November–December 2005.
- [22] S. Gezici, Z. Sahinoglu, H. Kobayashi, H. V. Poor, and A. F. Molisch, “A two-step time of arrival estimation algorithm for impulse radio ultrawideband systems,” in *Proceedings of 13th European Signal Processing Conference (EUSIPCO ’05)*, Antalya, Turkey, September 2005.
- [23] S. Gezici, Z. Sahinoglu, H. Kobayashi, and H. V. Poor, “Ultra wideband geolocation,” in *Ultrawideband Wireless Communications*, John Wiley & Sons, New York, NY, USA, 2005.
- [24] R. Merz, C. Botteron, and P. A. Farine, “Multiuser interference during synchronization phase in UWB impulse radio,” in *Proceedings of IEEE International Conference on Ultra-Wideband (ICU ’05)*, pp. 661–666, Zurich, Switzerland, September 2005.
- [25] S. Gezici, H. Kobayashi, and H. V. Poor, “A comparative study of pulse combining schemes for impulse radio UWB systems,” in *Proceedings of IEEE/Sarnoff Symposium on Advances in Wired and Wireless Communication*, pp. 7–10, Princeton, NJ, USA, April 2004.
- [26] S. Gezici, H. Kobayashi, H. V. Poor, and A. F. Molisch, “Optimal and suboptimal linear receivers for time-hopping impulse radio systems,” in *Proceedings of International Workshop on Ultra Wideband Systems; Joint with Conference on Ultra Wideband Systems and Technologies*, pp. 11–15, Kyoto, Japan, May 2004.
- [27] W. M. Lovelace and J. K. Townsend, “Chip discrimination for large near far power ratios in UWB networks,” in *Proceedings of IEEE Military Communications Conference (MILCOM ’03)*, vol. 2, pp. 868–873, 2003.
- [28] E. Fishler and H. V. Poor, “Low complexity multi-user detectors for time hopping impulse radio systems,” *IEEE Transactions on Signal Processing*, vol. 52, no. 9, pp. 2561–2571, 2004.
- [29] A. F. Molisch, K. Balakrishnan, D. Cassioli, et al., “IEEE 802.15.4a channel model—final report,” Tech. Rep., 2005, doc: IEEE 802.15-04-0662-02-004a. <http://www.ieee802.org/15/pub/TG4a.html>.
- [30] H. G. Şenel, R. A. Peters II, and B. Dawant, “Topological median filters,” *IEEE Transactions on Image Processing*, vol. 11, no. 2, pp. 89–104, 2002.
- [31] N. C. Gallagher Jr. and G. L. Wise, “Theoretical analysis of the properties of median filters,” *IEEE Transactions on Acoustics, Speech, and Signal Processing*, vol. 29, no. 6, pp. 1136–1141, 1981.
- [32] S. M. Kay, *Fundamentals of Statistical Signal Processing: Detection Theory*, Prentice Hall, Upper Saddle River, NJ, USA, 1998.
- [33] L. Yin, R. Yang, M. Gabbouj, and Y. Neuvo, “Weighted median filters: a tutorial,” *IEEE Transactions on Circuits and Systems II: Analog and Digital Signal Processing*, vol. 43, no. 3, pp. 157–192, 1996.

Zafer Sahinoglu received the B.S. degree in electrical engineering from Gazi University, Ankara, Turkey, in 1994, and the M.S. degree in biomedical engineering, and Ph.D. degree in electrical engineering (with awards) from the New Jersey Institute of Technology (NJIT), Newark, in 1998 and 2001, respectively. In 1999 he was with AT&T Shannon Research Labs. Since March 2001, he has been with Mitsubishi Electric Research Labs, Cambridge, Mass. His current research interests include MAC and upper-layer issues in wireless sensor networks, and ultra-wideband ranging, and geolocation. He has coauthored a book chapter on UWB geolocation and has authored and coauthored over 33 international journal and conference papers. He has contributed to MPEG21 standards on mobility modeling and characterization for multimedia service adaptation, to ZigBee on cost-aware routing and broadcasting, and to IEEE 802.15.4a standards on precision ranging. He is currently a Technical Vice-Editor in IEEE 802.15.4a TG and Chair of ZigBee industrial plant monitoring profile task group. He holds 11 patents.



Ismail Guvenc received the B.S. degree in electrical and electronics engineering from Bilkent University, Turkey, in 2001, and the M.S. degree in electrical and computer engineering from University of New Mexico, in 2002, and Ph.D. degree in electrical engineering from the University of South Florida in 2006. He was with Mitsubishi Electric Research Labs between January and August, 2005, where he worked on UWB ranging. Currently he is with DoCoMo USA Labs working on localization with UWB radios. His research interests are broadly in wireless communications and signal processing. In particular, he has worked on different aspects of UWB systems, such as ranging and localization, adaptive system design, transceiver types, channel parameter estimation, and multiuser communications. He is also interested in cognitive radio, wireless sensor networks, OFDM systems, and MIMO systems. He has published more than 20 conference and journal papers, and coauthored a book chapter. He has 4 pending US patent applications.

